JACS
JOURNAL OF THE AMERICAN CHEMICAL SOCIETY
Communication
pubs.acs.org/JACS

Role of Sodium Doping in Lead Chalcogenide Thermoelectrics

Jiaqing He,*[,†,#,⊥] Li-Dong Zhao,[‡,⊥] Jin-Cheng Zheng,[∥,⊥] Jeff W. Doak,[§] Haijun Wu,[†] Hui-Qiong Wang,[∥] Yeseul Lee,[‡] Chris Wolverton,[§] Mercouri G. Kanatzidis,*[,‡] and Vinayak P. Dravid[§]

[†]Frontier Institute of Science and Technology (FIST), Xi'an Jiaotong University, Xi'an 710054, P. R. China

[#]Department of Physics, South University of Science and Technology of China, Shenzhen 518055, P.R. China

[‡]Department of Chemistry and [§]Department of Materials Science and Engineering, Northwestern University, Evanston, Illinois 60208, United States

[∥]Department of Physics and Fujian Provincial Key Laboratory of Theoretical and Computational Chemistry, Xiamen University, Xiamen 361005, P. R. China

Supporting Information

ABSTRACT: The solubility of sodium and its effects on phonon scattering in lead chalcogenide PbQ (Q = Te, Se, S) family of thermoelectric materials was investigated by means of transmission electron microscopy and density functional calculations. Among these three systems, Na has the highest solubility limit (~2 mol %) in PbS and the lowest ~0.5 mol %) in PbTe. First-principles electronic structure calculations support the observations, indicating that Na defects have the lowest formation energy in PbS and the highest in PbTe. It was also found that in addition to providing charge carriers (holes) for PbQ, Na introduces point defects (solid solution formation) and nanoscale precipitates; both reduce the lattice thermal conductivity by scattering heat-carrying phonons. These results explain the recent reports of high thermoelectric performance in p-type PbQ materials and may lead to further advances in this class of materials.

The rock-salt-structured, narrow-band gap lead chalcogenide family of semiconductors (PbQ, Q = Te, Se, S) are of considerable scientific interest[1−6] because of their superior thermoelectric properties and potential applications in energy conversion.[7] The thermoelectric conversion efficiency of a material is related to the dimensionless quantity called the figure of merit, $ZT = \sigma S^2 T/\kappa$, where σ is the electrical conductivity, S is the Seebeck coefficient, T is the absolute temperature, and $\kappa = \kappa_e + \kappa_l$ is the total thermal conductivity, comprising electronic (κ_e) and lattice (κ_l) contributions. PbQ can be doped p-type by monovalent atomic substitutions on the Pb^{2+} sublattice. Na is one of the most effective dopants in controlling hole carriers in PbQ and has been extensively utilized to optimize their thermoelectric properties.[2] Historically, Na has been considered an ideal dopant that introduces hole carriers in PbQ with minimal effect on the other physical properties. Recently, however, our studies of the PbTe system showed that Na can contribute to the formation of nanoscale Na-rich precipitates beyond the solubility limit.[8]

In this work, we investigated two other important members of this family, PbSe and PbS, by employing advanced transmission electron microscopy (TEM) and theoretical calculations. Surprisingly, at Na doping levels of up to 2 mol %, we found solid solution behavior in PbS but nanoscale precipitates in PbSe. This suggests that the solubility limit of Na in the PbQ systems (beyond which nanoscale precipitates form) is a strong function of Q, which is supported by density functional theory (DFT) calculations. The value of κ_l calculated from the TEM observations suggests that these nanoscale precipitates also scatter heat-carrying phonons, albeit at the modest level of a solid solution (point defects). This is in contrast to other second-phase precipitates, which strongly scatter such phonons.[5] The new results and insights reported here enhance our understanding of the role of Na in p-type PbQ systems and should stimulate new ideas for designing more efficient p-type PbQ or $PbQ_{1-y}Q'_y$ (Q, Q′ = Te, Se, S; $0 < y < 1$) thermoelectric materials, particularly through optimization of the power factor (σS^2) and κ.

Details of the syntheses, characterization methods, property measurements, and thermoelectric properties are given in the Supporting Information (SI). TEM investigation of six samples of PbTe doped with 1 or 2 mol % Na (denoted as PbTe−x% Na), PbSe−y%Na (y = 1, 2), and PbS−z%Na (z = 0.5, 2) showed nanoscale precipitates in the first four samples and no nanoscale precipitates in PbS. On average, the number density of nanoparticles in the PbSe−2%Na sample was lower than in the PbTe−2%Na sample. Analyses along different crystallographic directions were used to obtain information about the precipitates' morphology and distribution. When the electron beam was parallel to the ⟨110⟩ or ⟨111⟩ zone axis, most of the precipitates appeared with a quasi-circular shape (pancake morphology), while when analyzed along the ⟨100⟩ zone axis, a high number density of precipitates also appeared as dark lines with lengths of a few nanometers. Therefore, most of the precipitates had a platelet-like shape, but there may have been a low number density of spherical-like precipitates, similar to those reported in K/Na-codoped PbTe.[8]

Figure 1a−c shows typical low-magnification TEM images of the samples with different directions indexed by the inserted electron diffraction (ED) patterns. In Figure 1a, a high density of circular nanoscale precipitates with dark contrast and a size distribution of 0.5−4 nm can be seen in the [011] direction for

Received: December 28, 2012
Published: February 27, 2013

   dx.doi.org/10.1021/ja312562d | J. Am. Chem. Soc. 2013, 135, 4624−4627

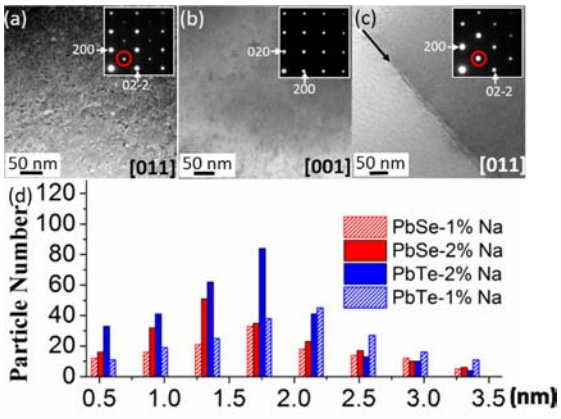

Figure 1. (a–c) Typical low magnification images and (insets) ED patterns for (a) [011] PbTe–2%Na, (b) [001] PbSe–2%Na, and (c) [011] PbS–2%Na. In (a), only one regular type of precipitate appears. In (b), there are two types: spherical-like and platelet-like. In (c), there are no precipitates. (d) Histogram of nanoscale precipitates in the studied samples taken from the same observation volume.

the PbTe–2%Na sample. Figure 1b shows a high number density of both circular and dark-line-shaped nanoscale precipitates in the [001] direction for the PbSe–2%Na sample. Figure 1c reveals the homogeneous nature of the PbS–2%Na material with no precipitates; the straight-line contrast feature marked by the black arrowhead reflects the presence of grain boundaries in the sample. Comparison of the ED patterns along [011] for the three PbQ samples showed that the relative intensity of (111) spot (circled in red) differs for the three samples: the I_{111}/I_{200} ratio for PbS is close to that for PbSe but much larger than that for PbTe. In principle, in the kinematic scattering approximation, the integrated intensity of any diffraction spot in the PbQ samples, *hkl*, can be expressed as:[9]

$$I_{hkl} = KH(\theta)|F_{hkl}|^2 \mathrm{LP}(\theta)\mathrm{TF}(\theta) \tag{1}$$

where K is a constant containing experimental factors associated with the geometry of the arrangement; $H(\theta)$ is the frequency factor for the particular plane; F_{hkl} is the structure factor, given by $F_{hkl} = f_{\mathrm{Pb}} + f_{\mathrm{Q}}e^{-2\pi i(hx+ky+lz)}$, in which the f_{Pb} and f_{Q} are atomic structure factors and x, y, and z are the atomic coordinates; $\mathrm{LP}(\theta)$ is the Lorentz and polarization factor; and $\mathrm{TF}(\theta)$ is the temperature factor. For the rock-salt structure, the I_{111}/I_{200} ratio is mainly related to the structure factor:

$$\frac{I_{111}}{I_{200}} \sim \frac{|F_{111}|^2}{|F_{200}|^2} = \frac{(f_{\mathrm{Pb}} - f_{\mathrm{Q}})^2}{(f_{\mathrm{Pb}} + f_{\mathrm{Q}})^2} \tag{2}$$

From the table of atomic scattering factors calculated by Gaussian expansion,[10] $(I_{111}/I_{200})_{\mathrm{PbTe}}$ is 0.08, which is 5 times smaller than the value of 0.46 for PbS.

Figure 1d shows the precipitate size distributions for the PbTe and PbSe samples using the same TEM observation volume. It is clear that the PbTe–*x*%Na samples have the higher densities of precipitates, ~1.5 times those of the corresponding PbSe samples. In all cases, the average particle size range was 0.5–3.5 nm. On average, the estimated (~5% error) distribution densities and sizes of all types of nanoscale precipitates were $\sim 0.8 \times 10^{12}$ cm^{-2} and ~1.5 nm for PbSe–2% Na and $\sim 1.2 \times 10^{12}$ cm^{-2} and ~1.8 nm for PbTe–2%Na, respectively. The estimated overall percentages of Na in the nanoscale precipitates in the PbTe and PbSe samples were smaller than their nominal values, which means that some Na dissolves into the matrix. This suggests that Na should completely dissolve in the matrix under a threshold percentage (~0.5 mol % for PbTe, ~0.9 mol % for PbSe, and ~2 mol % for PbS). These solubility limit estimates are based on the TEM study discussed later. Exceeding these limits results in the formation of nanoscale precipitates in the matrix.

To understand the trends in the Na solubility limit across the three PbQ systems, we used DFT[11,12] as implemented in the Vienna Ab initio Simulation Package[13] to calculate the dilute-limit solubility of Na in PbTe, PbSe, and PbS. Projector-augmented-wave (PAW)[14] pseudopotentials and the generalized gradient approximation of Perdew, Burke, and Ernzerhof[15] were used to calculate defect formation energies ($\Delta E_{\mathrm{F}}^{\mathrm{def}}$) for Na defects within the PbTe–NaTe, PbSe–NaSe, and PbS–NaS systems (for details, see the SI). $\Delta E_{\mathrm{F}}^{\mathrm{def}}$ for a Na solute in a PbQ compound is defined as

$$\Delta E_{\mathrm{F}}^{\mathrm{def}} = (E_{\mathrm{PbQ}}^{\mathrm{def}} - E_{\mathrm{PbQ}}^{\mathrm{pure}} - \mu_{\mathrm{Na}}^{0} + \mu_{\mathrm{Pb}}^{0}) - (\Delta\mu_{\mathrm{Na}} - \Delta\mu_{\mathrm{Pb}}) \tag{3}$$

where $E_{\mathrm{PbQ}}^{\mathrm{def}}$ is the DFT total energy of the PbQ supercell containing one Na atom; $E_{\mathrm{PbQ}}^{\mathrm{pure}}$ is the DFT total energy of the pure PbQ supercell; the quantities μ_{Na}^{0} and μ_{Pb}^{0} are the chemical potentials of Na and Pb in their standard metallic states, respectively; and the quantities $\Delta\mu_{\mathrm{Na}}$ and $\Delta\mu_{\mathrm{Pb}}$ are the changes in the chemical potentials of Na and Pb, respectively, due to the equilibrium between PbQ and NaQ, which are found from the compounds in thermodynamic equilibrium at the composition of the defect system. Substituting Na for Pb in PbQ puts the system on the pseudobinary tie line between PbQ and NaQ, so the equilibrium between these compounds can be used to determine the changes in μ_{Na} and μ_{Pb} relative to the elements.

Table S1 in the SI lists the $\Delta E_{\mathrm{F}}^{\mathrm{def}}$ values for one Na atom in 216 atom supercells of PbTe, PbSe, and PbS. $\Delta E_{\mathrm{F}}^{\mathrm{def}}$ is positive for PbTe but negative for PbSe and PbS. The negative values suggest the presence of as-of-yet-unknown ternary compounds in the Na–Pb–Se and Na–Pb–S systems, which would alter the conditions of equilibrium, raising $\Delta E_{\mathrm{F}}^{\mathrm{def}}$ for Na on Pb in PbSe and PbS. Qualitative evidence for a ternary phase in the Na–Pb–S system has been presented previously.[16] From the positive value of $\Delta E_{\mathrm{F}}^{\mathrm{def}}$ for Na in PbTe, the dilute-limit solubility of Na in PbTe [given by $x_{\mathrm{Na}}^{\mathrm{PbTe}}(T)$, the mole fraction of Na replacing Pb in PbTe at temperature T] was calculated to be 0.6 mol % at 600 K using the equation

$$x_{\mathrm{Na}}^{\mathrm{PbTe}}(T) = e^{-\Delta E_{\mathrm{F}}^{\mathrm{def}}/k_{\mathrm{B}}T} \tag{4}$$

where k_{B} is Boltzmann's constant.

Despite the negative values of $\Delta E_{\mathrm{F}}^{\mathrm{def}}$ for Na in PbSe and PbS, we can make the following qualitative statements regarding the trends in PbQ–NaQ pseudobinary systems. First, the defect formation energy with respect to the elements (the first term of in eq 3) decreases as the anion is varied from Te to Se to S. This defect formation energy of Na in PbS is twice the magnitude of that for Na in PbTe. The trend seen in the "raw" defect formation energies persists in the defect formation energies with respect to the compounds PbQ–NaQ (i.e., $\Delta E_{\mathrm{F}}^{\mathrm{def}}$), which become more negative as the anion is changed from Te to Se to S. We hypothesize that the predicted ternary compounds in the Pb–Na–Se and Pb–Na–S systems would result in positive $\Delta E_{\mathrm{F}}^{\mathrm{def}}$ values but would not qualitatively alter the trend in the energetics, which is in qualitative agreement

dx.doi.org/10.1021/ja312562d | J. Am. Chem. Soc. 2013, 135, 4624–4627

with the experimentally observed trends in the Na solubility limits across the PbQ systems.

To determine the microstructural features of the nanoscale precipitates and analyze the strain distribution at the boundaries between the precipitates and the PbQ matrix, we examined all six samples at the atomic level using high-resolution TEM (HRTEM). A representative HRTEM image of PbS−2%Na obtained with the electron beam parallel to the [011] axis did not show any nanoscale precipitates (Figure 2a).

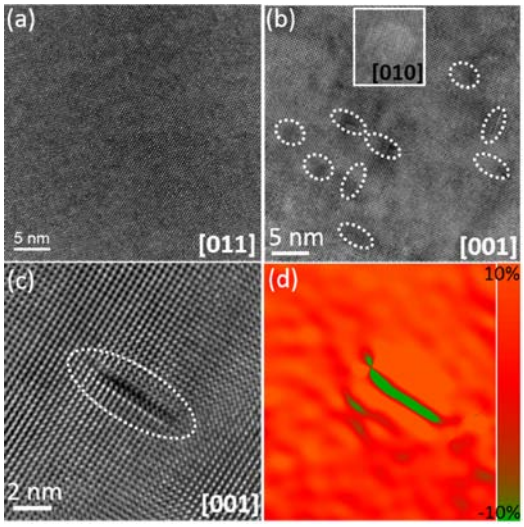

Figure 2. (a) Typical lattice image of the [011] PbS−2%Na sample. (b) High-magnification atomic image of [100] PbSe−2%Na depicting some perpendicular or parallel platelet-like precipitates and spherical precipitates. The inset shows a small square precipitate having a coherent interface with the matrix. (c) Lattice image and (d) strain map showing elastic strain along only one direction for the platelet-like precipitates.

Therefore, the sample was clearly a solid solution. Figure 2b and its inset show high-magnification lattice images of PbSe−2%Na along the [001] and [010] directions, respectively. Both images depict a high density of weak-contrast nanoscale circular and dark-line-shaped precipitates. The projections of the circular precipitates revealed a higher number density than the linear ones. In the lattice image taken along the [001] direction shown in Figure 2c, one dark line can clearly be observed.

To analyze the possible strain at or close to the precipitate−matrix interface, some regular platelet-like shaped precipitates were studied by geometric phase analysis (GPA),[17] which is a method of HRTEM image processing for strain-field analysis. Some precipitates showed negligible strain at the boundaries, while others showed under relative 10% strain along a certain direction. Figure 2d shows a GPA strain map along the ε_{xx} direction, which clearly shows strain in the x direction. However, GPA did not find measurable strain in the y direction (data not shown). Thus, the strain associated with these precipitates exists along only one of the ⟨100⟩ directions. Therefore, the strain distribution in platelet-like precipitates is anisotropic, in contrast to spherical precipitates, which exhibit a relatively "homogeneous" omnidirectional strain distribution. From the precipitate composition, a mass density of ∼7.6 g/cm^3 can be calculated for the precipitates in the PbSe−2%Na sample. This value is lower than that for pure PbSe (∼8.27 g/cm^3).

To understand the effect of Na addition on κ_l of PbQ and the mechanisms of phonon scattering, semiclassical theoretical calculations based on the modified Callaway model were conducted (for details, see the SI).[18] Only the relaxation time (τ_c) is shown here. At a given frequency, τ_c is given by:

$$\tau_c^{-1} = \tau_U^{-1} + \tau_N^{-1} + \tau_D^{-1} + \tau_S^{-1} + \tau_{PD}^{-1} + \tau_P^{-1} \quad (5)$$

where τ_U, τ_N, τ_D, τ_S, τ_{PD}, and τ_P, are the relaxation times corresponding to scattering from Umklapp processes, normal processes, dislocations, strains, point defects, and precipitates, respectively (for details on each term, see the SI). The first two contributions originate mainly from the matrix. In the present results, strains and dislocations at the boundaries between the precipitates and the matrix were observed. However, their number densities were low, so they were not considered in our calculations. The last two terms, giving the contributions of point defects (solid solution) and precipitates, largely scatter phonons. The point defects are mainly the dissolved Na ions in the matrix; precipitate scattering is related to the density and size of the nanoscale particles embedded in the matrix.

Based on the formulas and the parameters obtained from the TEM observations (Tables S2 and S3), the κ_l values for three typical samples of PbQ−2%Na were calculated. To assess the reliability of the calculations, we directly compared the calculated values to the experimentally derived ones (Figure 3a) and obtained very good agreement (within 10% error

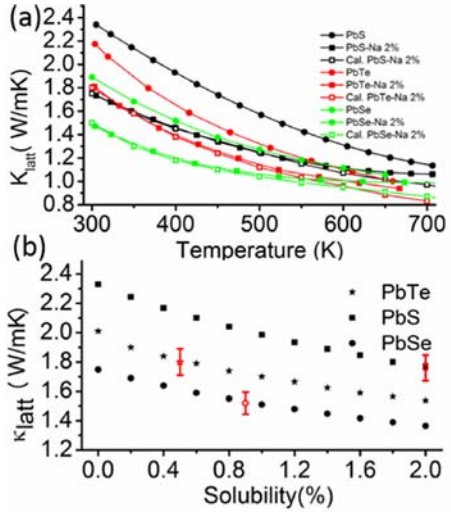

Figure 3. (a) Temperature dependence of the lattice thermal conductivity for three typical PbQ−2%Na samples plus a pure PbQ sample with calculated Lorenz number. Open symbols were obtained from theoretical calculations based on TEM observations. (b) Solubility dependence of the lattice thermal conductivity of PbQ−2%Na samples at room temperature. Error bars on measured data are shown in red.

below ∼550 K). This indicates that the proposed model involving theoretically and experimentally derived parameters is appropriate for this combined nanostructure/solid solution system. Above 550 K, the deviation between the calculated and experimental results has two main causes: (1) the over-estimation in the obtained experimental results as a result of the contribution of bipolar diffusion when electrons and holes both are present at high temperature[19] and (2) the assumption that the solubility limit of Na is independent of temperature, which is most likely incorrect. In fact, some Na in the precipitates

dx.doi.org/10.1021/ja312562d | J. Am. Chem. Soc. 2013, 135, 4624−4627

dissolves into the matrix at high temperature, and the solubility limit consequently increases. Therefore, the average size and number density of nanoscale precipitates at high temperature should be smaller than those at low temperature, and the number density of point defects should be larger.[20] Our calculations also indicate that point defects as well as dislocations scatter high-frequency phonons (those with short mean free paths), while nanoscale precipitates play an important role in scattering of low-frequency phonons (ones with intermediate or long mean free paths).

To estimate the solubility limit at room temperature for $Pb_{1-x}Na_xQ$ compositions, we calculated the percentage of nanoscale precipitates using the average sizes and number densities obtained by the TEM studies. The solubility (x) was in the range 0.001−0.020, resulting from the disparity between the calculated Na mole percent and the nominal composition. To illustrate the significance of the point defect effect, Figure 3b demonstrates that κ_l decreases with increasing x and also reveals that the solubility limits for PbTe, PbSe, and PbS are ∼0.5, ∼0.9, and ∼2 mol %, respectively. A solubility range instead of an exact number is given because it was difficult to measure the average solubility of the whole specimen using localized TEM observations. All of the samples studied with the aforementioned model exhibited similar results, namely, a κ_l value different from that of pristine PbQ, which means Na itself reduces κ_l. These results can readily account for the experimental data of Pei et al.,[2] who found different values of κ_l for 1 and 2 mol % Na in $PbTe_{1-x}Se_x$ samples.

We conclude that Na-doped PbQ samples, which previously were believed to be single-phase materials with dissolved Na, contain a combination of point defects (solid solution) and nanoscale architectures. These features occur at thermoelectrically relevant concentrations of Na exceeding a certain percentage (0.5 mol % for PbTe, 0.9 mol % for PbSe, and 2 mol % for PbS). The experimentally observed trends in the solubility limits of Na in PbQ were qualitatively captured by DFT calculations of the defect formation energies for Na in PbQ. The TEM studies and theoretical calculations revealed that the platelet-like nanoscale precipitates do not result in strong impedance as a result of strong phonon scattering because their crystallographic structure and mass density are close to those of the PbQ matrix. Compared with other second phases such as SrQ, these nanoscale precipitates scatter long-wavelength phonons much more weakly.[1,5] Nevertheless, point defects and precipitates in these Na-doped systems can still reduce κ_l to some extent. These findings shed new light on our understanding of high-performance p-type lead chalcogenides and can guide continued advances in their performance.

■ ASSOCIATED CONTENT

Ⓢ Supporting Information

Experimental details, characterization data, calculations, and complete ref 16. This material is available free of charge via the Internet at http://pubs.acs.org.

■ AUTHOR INFORMATION

Corresponding Author

he.jq@sustc.edu.cn; m-kanatzidis@northwestern.edu

Author Contributions

⊥J.H., L.-D.Z., and J.-C.Z. contributed equally.

Notes

The authors declare no competing financial interest.

■ ACKNOWLEDGMENTS

This work was supported as part of the Center for Revolutionary Materials for Solid State Energy Conversion, an EFRC funded by the U.S. Department of Energy, Office of Science, Office of Basic Energy Sciences under Award DE-SC0001054, and was also supported in part by the 973 Program of the Ministry of Science and Technology of China (Grant 2012CB619401 to J.H.). The portion of the calculations done at Xiamen University was supported by the National Natural Science Foundation of China (Grant U1232110).

■ REFERENCES

(1) Biswas, K.; He, J.; Blum, I. D.; Wu, C.-I.; Hogan, T. P.; Seidman, D. N.; Dravid, V. P.; Kanatzidis, M. G. *Nature* **2012**, *489*, 414.

(2) (a) Pei, Y. Z.; Shi, X. Y.; LaLonde, A.; Wang, H.; Chen, L. D.; Snyder, G. J. *Nature* **2011**, *473*, 66. (b) Girard, S. N.; He, J.; Zhou, X.; Shoemaker, D.; Jaworski, C.; Uher, C.; Dravid, V. P.; Heremans, J. P.; Kanatzidis, M. G. *J. Am. Chem. Soc.* **2011**, *133*, 16588. (c) Rogers, L. *J. Phys. D: Appl. Phys.* **1968**, *1*, 1067. (d) Sootsman, J. R.; Pcionek, R. J.; Kong, H.; Uher, C.; Kanatzidis, M. G. *Chem. Mater.* **2006**, *18*, 4993.

(3) (a) Wang, H.; Pei, Y. Z.; LaLonde, A. D.; Snyder, G. J. *Adv. Mater.* **2011**, *23*, 1366. (b) Zhang, Q.; Cao, F.; Liu, W.; Lukas, K.; Yu, B.; Chen, S.; Opeil, C.; Broido, D.; Chen, G.; Ren, Z. *J. Am. Chem. Soc.* **2012**, *134*, 10031.

(4) Wang, H.; Pei, Y.; LaLonde, A. D.; Snyder, G. J. *Proc. Natl. Acad. Sci. U.S.A.* **2012**, *109*, 9705.

(5) (a) Zhao, L.-D.; Lo, S.-H.; He, J.; Li, H.; Biswas, K.; Androulakis, J.; Wu, C.-I.; Hogan, T. P.; Chung, D.-Y.; Dravid, V. P.; Kanatzidis, M. G. *J. Am. Chem. Soc.* **2011**, *133*, 20476. (b) Biswas, K.; He, J.; Zhang, Q.; Wang, G.; Uher, C.; Dravid, V. P.; Kanatzidis, M. G. *Nat. Chem.* **2011**, *3*, 160.

(6) Androulakis, J.; Todorov, I.; He, J.; Chung, D.-Y.; Dravid, V.; Kanatzidis, M. *J. Am. Chem. Soc.* **2011**, *133*, 10920.

(7) (a) Snyder, G. J.; Toberer, E. S. *Nat. Mater.* **2008**, *7*, 105. (b) Kanatzidis, M. G. *Chem. Mater.* **2010**, *22*, 648. (c) Vineis, C. J.; Shakouri, A.; Majumdar, A.; Kanatzidis, M. G. *Adv. Mater.* **2010**, *22*, 3970.

(8) He, J.; Androulakis, J.; Kanatzidis, M. G.; Dravid, V. P. *Nano Lett.* **2012**, *12*, 343.

(9) Ehrhardt, C. H.; Horovitz, K. L. *Phys. Rev.* **1940**, *57*, 603.

(10) Vand, V.; Eiland, P. F.; Pepinsky, R. *Acta Crystallogr.* **1957**, *10*, 303.

(11) Hohenberg, P.; Kohn, W. *Phys. Rev.* **1964**, *136*, 864.

(12) Kohn, W.; Sham, L. J. *Phys. Rev.* **1965**, *140*, 1133.

(13) Kresse, G.; Furthmüller, J. *Phys. Rev. B* **1996**, *54*, 11169.

(14) Blochl, P. E. *Phys. Rev. B* **1994**, *50*, 17953.

(15) Perdew, J.; Burke, K.; Ernzerhof, M. *Phys. Rev. Lett.* **1996**, *77*, 3865.

(16) He, J.; et al. *Nano Lett.* **2012**, *12*, 5979.

(17) Hytch, M. J.; Snoeck, E.; Kilaas, R. *Ultramicroscopy* **1998**, *74*, 131.

(18) Callaway, J.; von Baeyer, H. C. *Phys. Rev.* **1960**, *120*, 1149.

(19) Kitagawa, H.; Wakatsuki, M.; Nagaoka, H.; Noguchi, H.; Isoda, Y.; Hasezaki, K.; Noda, Y. *J. Phys. Chem. Solids* **2005**, *66*, 1635.

(20) He, J.; Sootsman, J. R.; Girard, S. N.; Zheng, J.-C.; Wen, J.; Zhu, Y.; Kanatzidis, M. G.; Dravid, V. P. *J. Am. Chem. Soc.* **2010**, *132*, 8669.